Laser Induced Breakdown Spectroscopy technique for the detection of major elements in Particulate Matter from in-use Petrol engine Passenger vehicles.

By

Muhammad Bilal Anjum

Supervised By

Prof. Dr. Raheel Ali

Registration Number: 02182113027

Department of Physics Quaid I Azam University Islamabad.

2023

This work is submitted as a dissertation as a partial fulfillment of the requirement for the degree of

MASTER OF PHILOSOPHY

IN

PHYSICS

TO THE

DEPARTMENT OF PHYSICS

QUAID I AZAM UNIVERSITY

ISLAMABAD, PAKISTAN

2023

Dedicated To

My Beloved Parents

Teachers

Siblings

&

And Friends

ACKNOWLEDGMENT

All praises to Allah Almighty, who enabled me to achieve the milestone of my academic career. Countless Blessings of Allah be upon His most beloved and last Prophet; The supreme repository of wisdom for humanity is Hazrat Muhammad (S.A.W.W.).

First and foremost, I am extremely grateful to my research advisor, Prof. Dr. Raheel Ali, for his kind guidance and for allowing me to research at the Atomic and Molecular Spectroscopy Laboratory.

Also, many thanks to my lab mates Akhtar Muhammad, Jamil, and Mohsin, who supported me, guided me, and cooperated with me in the lab.

I sincerely thank my parents and siblings, who supported and encouraged me at each step of my life.

Certificate

It is acknowledged that the work in this thesis was done in the Atomic and Molecular Spectroscopy Laboratory under my supervision, Department of Physics, Quaid-i-Azam University, Islamabad, Pakistan.

Submitted through

_____

Prof. Dr. Kashif Sabeeh,

Chairman Department of Physics,

Quaid I Azam University Islamabad.

Supervised By

_____

Prof. Dr. Raheel Ali

Department of Physics,

Quaid I Azam University Islamabad.

Contents

Abstract

The primary concern of this study offers a critical understanding of the basic composition of petrol particulate matter (PPM) from In-use engine passenger vehicles, which can aid in developing the doable ways to reduce the air pollution, these vehicles release.Successful application of Laser-Induced Breakdown Spectroscopy (LIBS) for the elemental analysis of Petrol Particulate matter from In-use Petrol Engine Passenger vehicles has been performed. A 532nm Nd: YAG laser was used to create the plasma plume, and a fice channel HR 2000 Spectrometer covering the wavelength range from 200-700nm was used to record the spectra of the plasma plume. By using the online NIST database, the spectral lines are observed. Before the quantitative analysis, the Boltzmann equation and the Stark Broadening line profile were used to determine the electron temperature and number density.

The slope of the Boltzmann plot was used to determine the electron temperature. The stark broadening effect was employed to calculate the electron number density; Vogt fitting was used to calculate the entire width at half maximum for the stark broadened line. The quantitative analysis was performed using the calibration-free method, revealing that Ca and Fe are the major elements in the Particulate matter sample. The concentration of other elements like Na, Li, Mg, and Ni are also present in the Particulate Matter Sample.

Chapter#1

Introduction

1.1 Spectroscopy:

Atomic and molecular physics began gaining significant scientific interest at the turn of the 20th century. The foundation for this significant and vast area of spectroscopy was created by renowned spectroscopists Rydberg and Balmer[i]. The investigation of these interactions is known as spectroscopy. This is one of the best scientific approaches to studying the natural world. Because of this, it demonstrates both the intrinsic and extrinsic properties of matter. It entails exposing a substance to radiation to discover more about the substance's qualities. Different radiation sources offer different information and are used to evaluate different compounds. Spectroscopy may use the distinctive identification of a material to examine it by examining the elements it contains and their concentrations. The interaction between Earth and the sun normally involves no physical activity. This amazing scientific technique may also reveal information on atoms, molecules, and even the smallest atom-forming particles[ii]. At first, only visible light was used to study the atomic structure or a sample qualitatively and quantitatively. However, in our modern technological era of research, certain advanced methods for the spectroscopic investigation of materials have been devised. Electromagnetic radiation can be employed in this application, with examples including UV, X-rays, and infrared radiation.

1.1.2 Spectroscopy's early development:

After discovering that white light disperses into seven different hues when it passes through a prism, Sir Isaac Newton developed spectroscopy. William Wollaston developed the original spectrometer in 1802, which it utilized to concentrate the sun's spectrum onto a screen. Wollaston noticed that the sun's colour spectrum was not uniform and that eight hue patches were missing. Fraunhofer independently identified emission and absorption lines in the flames and sun spectra in 1817. Fraunhofer invented the electroscope in 1814. According to a theory

developed in 1859 by Bunsen and Kirchhoff, each element has its spectrum. According to Kirchhoff, three laws control spectroscopy:

Any source observed through a cool, low-density gas will yield an emission line spectrum. Under high pressure, continuously varying wavelengths are emitted by incandescent solids, gases, or liquids. The ability of hot gas to emit "bright lines" of emission line spectra when under low pressure.

The development of quantum mechanics led to significant advances in the theoretical aspects of spectroscopy in the 1920s and 1930s. As a result, spectroscopy and quantum mechanics started to resemble one another[iii]. Experimental precision has risen with the invention of various novel spectroscopic techniques, particularly the dye laser innovation.

1.1.3 Applications of spectroscopy:

- Spectroscopy has allowed scientists to investigate novel research fields theoretically and experimentally. Here are a few examples of spectroscopy applications:
- Emission or absorption spectroscopy is incredibly useful for a quantitative study of the sample to establish the volume of the material in a sample.
- Spectroscopy is widely applied in biochemistry, biological research, and medicine.
- Astrophysicists use the atomic spectrum to ascertain the physical characteristics of distinct things. Additionally useful in remote sensing is spectroscopy.
- Applications of modern spectroscopy include optical astronomy, accurate frequency measurements, and atomic cooling.
- The majority of studies on the elements in body fluids use spectroscopy.

1.1.4 Introduction to laser:

The light amplification by stimulated emission of radiation (LASER) technique produces a strong, coherent, collimated, and monochromatic electromagnetic radiation beam. With this technique, a second photon stimulates the emission of an excited atom, and the two photons travel in the same direction to create coherent, monochromatic light.

1.1.5 Multilevel laser system:

There are two energy levels in the basic understanding of laser activity. However, the laser mechanism should entail more than two energy levels.

i. Three-Level Laser systems:

This system has three energy levels (E_1, E_2, and E_3), one of which is a metastable state. This makes it easier for the populace to switch between the two energy levels. To decay back to E_2, a metastable state, electrons are pumped from E to E_3, where they stay briefly before doing so[iv]. This makes it possible to start a lasing action and ensures that there will be a population inversion between E_1 and E_2.

ii. Four Level Lasing System:

This system has four distinct energy levels, referred to as E1, E2, E3, and E4, respectively. E4 provides temporary nonradioactive decay. E4 is filled with excited electrons from E. They return surprisingly quickly to E3, a metastable state with a longer lifetime than others. The population inversion between E3 and E2 is responsible for the lasing activity.

1.2 Atomic Spectroscopy:

"Spectroscopy" refers to the study of emission or absorption spectra. The best method for figuring out an element's makeup is this. Three other subcategories of spectroscopy are atomics mass (AMS), atomic absorption (AAS), and emission spectroscopy (AES). Each element's spectrum is unique because of its unique electrical structure. The fundamental function of spectroscopy is the analysis of absorption and emission spectra. The emission wavelengths of the light are shown on the spectrum together with their corresponding counts and intensities. The photon energy emitted or taken in has been determined as below.:

$$hv = E_2\text{-}E_1.$$

E_2 and E_1 are the higher and lower energy levels in the equation.

.

1.2.1 Atomic Absorption Spectroscopy:

In this procedure, the sample's absorption spectra are analyzed. A photon of a certain wavelength is absorbed in the sample when continuous radiation passes over it by the electrical structure of the material. The elements can be recognized by examining the spectrum of the transmitted light.

1.2.2 Atomic emission spectroscopy:

We employ this method to study the material's optical emission spectra. Initially, an electrical discharge source that can be seen is used to stimulate the sample to greater energy levels. Atoms are elevated to higher energies. They gradually decay to lower energy levels (stable states) when they release the energy photons they have absorbed. The electrical structure of the parts affects the wavelengths of the generated photons. An optical spectrometer is used to detect the photons' wavelengths. These wavelengths could belong to the infrared, X-ray, or visible spectrum. We could produce an optical fingerprint of the components of the sample by looking at these wavelengths. Every sample has a distinctive fingerprint, which allows for identification[v].

1.2.3 Atomic Mass Spectroscopy:

Mass spectroscopy is the scientific method used to examine the mass distribution of a given sample. The elements are put through an magnetic and electric field from the outside. Based on the charge-to-mass ratios of the elements, these fields divide them. The magnetic field gives the elements circular trajectories while the electric field accelerates them. These routes adhere to the equation: r = mv/qb, where q is the element's charge, v is its speed, and b is the applied magnetic field. Heavy and lighter elements' paths will differ by the relationship mentioned above. The isotopes of several elements are separated using this spectroscopy. Isotopes have various masses, which causes them to follow different paths in the electric and magnetic fields. They are divided as a result.

1.3 Laser-induced Breakdown Spectroscopy (LIBS):

Examining the optical emission spectrum is a component of the procedure referred to as laser-induced breakdown spectroscopy (LIBS). This is an excellent technique for examining the substance in all three states—solid, liquid, and gas. There is no need to prepare a sample beforehand. This process is speedier than prior approaches to spectroscopy, and it is also more effective and less expensive than those procedures. LIBS has applications in virtually every field of science. A LIBS has recently undergone some exciting advances that have made it possible to investigate distant targets remotely. This helps in the analysis of materials that have the potential to be explosive or harmful. As a result, space exploration has grown easier. LIBS may be subject to limitations under certain conditions. In many cases, the extent of the analysis is constrained by the amount of laser power being utilized. It's possible that the target sample won't be sufficiently excited by a single laser shot. By doing this, the sample might avoid getting stimulated and atomized. As a result, we must select the laser's energy carefully. The environment of the sample also has an impact on LIBS spectroscopy. Despite all these limitations, researchers routinely make use of this methodology. Finally, it has been shown that LIBS is a very promising method for a range of materials[vi].

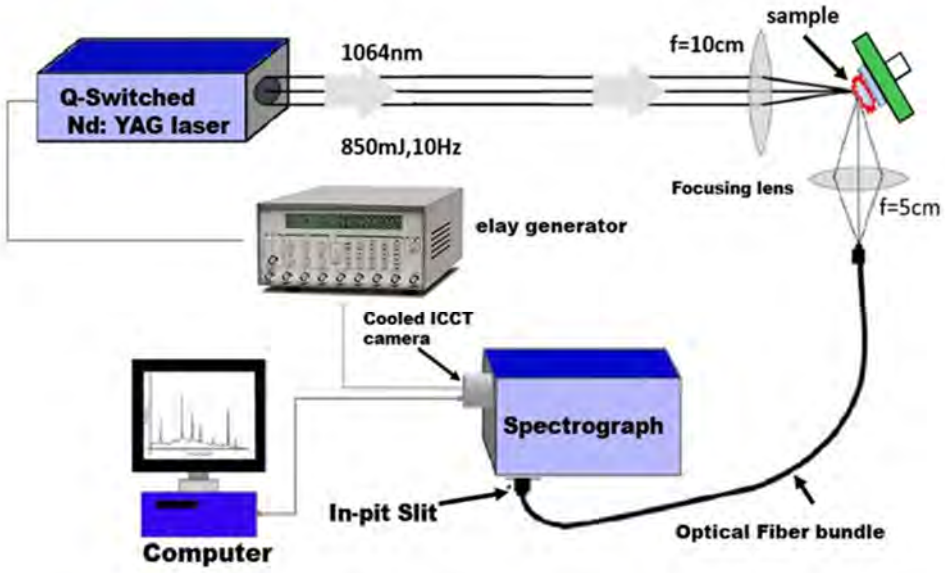

Figure 1. 1 Schematic Diagram Of LIBS setup

1.3.1 Basic principles of LIBS:

Fundamental to the operation of LIBS is the excitation and de-excitation of the sample being studied. When stimulating a target, a laser is employed as the excitation source. The target sample produces plasma[vii]. As plasma de-excites, photons are released. Since each element produces radiation at a different frequency, these radiations are recorded using an optical spectrometer. This spectrometer is sensitive enough to detect and record every wavelength of radiation emitted by the plasma. By studying the characteristics of emitted wavelength we can identify the element of sample.

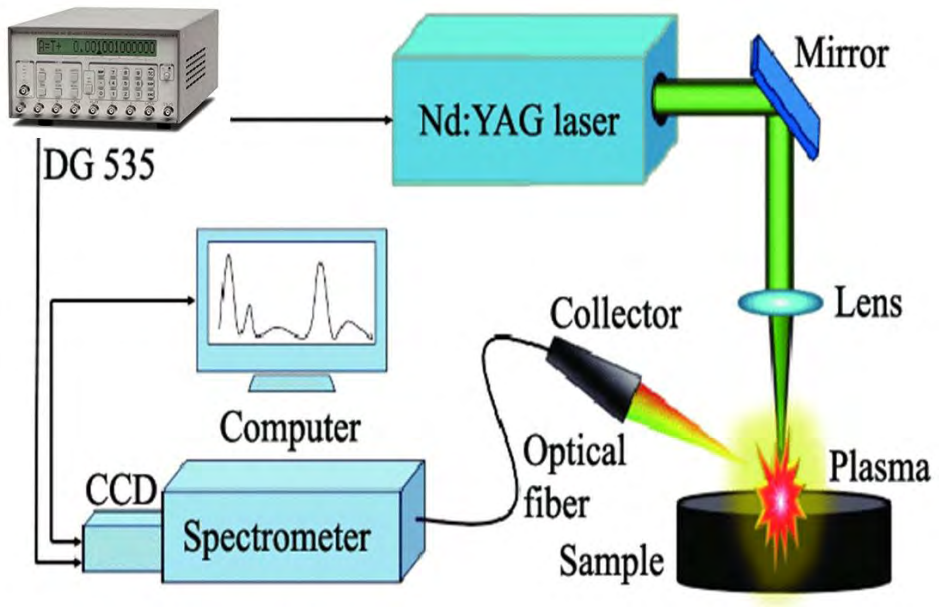

Figure 1. 2 shows the pulsed LIBS analysis setup schematic diagram.

1.3.2 Target Ablation:

While the laser beam concentrates on a small target area, numerous actions could happen on the surface of the target. Several elements like laser power, pulse duration, spot size, and sample type might influence these reactions. Some significant phenomena are characterized as follows:

i. The energy of the laser light is transmitted to the atoms by collisions, raising the sample's temperature. This method turns laser energy into thermal energy. Vibrations in the lattice transport the thermal energy to the sample matrix. The target melts and vaporizes more quickly as the sample's temperature rises. Photothermal ablation is the term used to describe this mechanism.

ii. A few atoms might absorb some energy and become excited. Electrons can jump from lower energy levels to higher energy levels (Excited states). This occurs when the laser energy is strong enough to ionize the sample, such as using a femtosecond laser. The atoms are usually ionized due to energy absorption, and the resulting electron jumps to higher states. This is called photochemical ablation.

iii. There is a third method of ablation, which combines the first two methods. Free electrons are generated during the photochemical reaction. The laser energy is delivered to the matrix by these

electrons as they move through it photochemically. The material is vaporized and ablated as a result[viii].

1.3.3 Post Ablation Process:

The interaction between a laser and the target when it is pointed at it is very intricate. Many different occurrences are taking place, each of which is complicated. The leading edge of the laser's beam shines on the material's surface, releasing energy into its atoms[ix]. The material is ablated when the threshold energy for ablation equals the laser energy per shot. After the target has been ablated, most of the material is converted into vapors, predominantly of neutral atoms and electrons. Following the abolition of some material, the trailing edge of the laser beam will now interact with the remaining substance. These vapors and electrons ingest the laser energy and get ionized. Ionization is increased to a significant degree in the plasma that is created all around the surface of the target.

1.4 Plasma:

The term "plasma" refers to a highly ionized gas of ions and electrons and exhibits the collective behavior of a quasi-neutral gas of charged and neutral particles. Plasma is created when a gas is ionized to a very high degree.

> "A quasi-neutral gas of charged and neutral particles that exhibits a collective behavior is called plasma."

Plasma is composed of electrons, ions, and neutral atoms. In some plasma regions, the concentration of charged particles, such as ions or electrons, may be higher than in other regions, indicating the plasma's charge character[x]. However, the number density of ions and electrons in the plasma is roughly equal ($n_i=n_e$), indicating the plasma's overall neutral behavior. To put it another way, an observer who is located within the plasma will notice that they are a cluster of charged particles surrounding them observer who is located outside of the plasma will notice that the plasma can be upset by an electric field, a magnetic field, or some other force. The plasma will react to the disturbance. Collective conduct is the term used to describe this characteristic.

Conductance is an additional essential quality of plasma; as an ionized gas with free charge carriers, plasma performs very well as a conductor due to its exceptional electrical properties.

1.4.1 Plasma Expansion:

When plasma is just beginning to develop, the material is strongly ionized and has reached very high temperatures. The plasma temperature is typically somewhere between 100,000 and 100,000 K for most of the time. At these extremely high temperatures, plasma can emit radiation in a continuous spectrum. This spectrum does not lend itself well to identifying composition meaningfully. The plasma expands over time and finally becomes cooler. As the temperature continues to fall, it reaches 4,000 -2000 K. Currently, plasma generates the characteristic frequencies of the various elements present in the system. To record this radiation, an optical spectrometer is utilized. The LIBS method is based on this fundamental idea as its guiding premise[xi].

1.4.2 Plasma Parameter:

Plasma cannot be used to refer to either of these ionized gases. Ionization is something that can never be completely absent from a gas. To be considered gas, a substance must fulfil all three of the following prerequisite conditions and qualities:

1. $\lambda_D << L$
2. $N_D >> 1$
3. $\omega\tau >> 1$

Where Nd is the Debye sphere's particle count, which can be expressed as:

$$N_D = n \frac{4}{3} \pi \lambda D^3 \qquad (1.1)$$

i. The Debye length, denoted by D, should be significantly shorter than the dimensions of the plasma container. Because of this necessity, it is ensured that any potential source from the outside that is brought into the plasma will be blocked off in a region that is significantly smaller than the chamber itself.

ii. The number of particles (N_D) should be within the Debye sphere, which shows the behavior of the plasma species as a group[xii].

The symbol marks the oscillation frequency of the plasma, and the symbol represents the mean relaxation period that occurs in between collisions with neutral atoms. Because of this requirement, it is essential for electromagnetic forces, rather than the more traditional hydrodynamic forces, to regulate plasma motions.

1.5 Plasma Characterization in LIBS:

Because emission lines give significant information about LIBS, characterization of the plasma is the most crucial part of methods of plasma spectroscopy. Plasma characterization provides information on the number density and the temperature of the plasma. This section offers a concise overview of the methodologies used to compute the number density and plasma temperature.

1.5.1 Assumptions in the Plasma Characterization:

Because emission lines give significant information about LIBS, characterization of the plasma is the most crucial component of the many techniques of plasma spectroscopy. Plasma characterization can provide information on the number density and the plasma temperature. This section offers a concise breakdown of the methodologies behind determining the plasma temperature and number density[xiii].

1.5.2 Local Thermo-Dynamical Equilibrium (LTE):

To calculate the temperature of plasma, it is necessary to use not one but two of the most well-known equations for equilibrium. The first Boltzmann equation, which describes the amount of energy possessed by the population as a function of the surrounding temperature, is denoted by the formula.

$$\frac{N_j^Z}{N^z} N^z = g_j \; e^{\frac{-E_j^Z}{KT}} \qquad (1.2)$$

In this equation, the subscript "z" stands for the ionization stage (z = 0 for neutral and z = 1 for singly ionized ions), Nz stands for the number density, Ej stands for the energy of the level, gj stands for the energy degeneracy, UZ(T) stands for the partition function, and k stands for the Boltzmann constant. The second equation is known as the Saha–Boltzmann equation, and it is used to describe the densities of the ionization species that are a function of temperature. i.e.:

$$\frac{N_e N_z}{N^{z-1}} = 2\frac{U^z(T)}{U^{Z-1}(T)}\left[\frac{2\pi mkT}{h^2}\right]^{\frac{3}{2}} e^{\frac{E_\infty^{Z-1}-\Delta E_\infty^{Z-1}}{KT}} \qquad \textbf{(1.3)}$$

Where h represents the constant of Planck, UZ (T) represents the partition function, m represents the mass of an electron, and Ne represents the electron number density. The ionization energy of the Z-1 states, also known as EZ-1, is considered the most reliable indicator of local thermodynamics. To employ these two equations, you must first achieve equilibrium, a required condition. In a state of local thermodynamic equilibrium, all species, including neutral particles, ions, and electrons, are subjected to the same temperature. Utilizing statistical methods to investigate the workings of the entire system is a straightforward process. LTE is another piece of evidence that supports Kirchhoff's law of radiation[xiv]. i.e.$\frac{\varepsilon_{\lambda(\lambda)}}{k'(\lambda)} = B_\lambda(\lambda, T)$

(1.4)

In this equation, $B_\lambda\ (\lambda, T)$ represents the intensity of the blackbody radiation at temperature T. In order to keep the local thermodynamic equilibrium (LTE), the radiative process needs to be pushed by collisions between electrons. For this scenario to play out, there must be a minimum electron density of around 101 cm. Mc Whirter developed a criterion that ensures LTE for the threshold electron density value. i.e.:

$$N_e \geq 1.6(10)^{12}(T^2)(\Delta E^3)\, cm^{-3} \qquad \textbf{(1.5)}$$

Where T (K) is the excitation temperature and ΔE (eV) is the greatest energy gap between the transition levels.

1.5.3 Optically thin spectral line emission:

When computing the plasma characteristics (Excitation temperature and electron number density), the optically thin spectral line emission status is also considered as part of the process. If one wishes to use the dramatic broadening effect to compute the electron number density and ascertain the temperature of the plasma using the Boltzmann and Saha equations, the emission lines in question have to be optically thin. This suggests that the lines do not demonstrate any characteristics of self-absorption; they are not saturated; they do not demonstrate any characteristics of distorted areas or widths. If this criterion is not satisfied, then the electron number density and plasma temperature estimates will be erroneous. It is possible to establish the existence of optically thin spectral line emission by utilizing the relative strength of the emission lines that have been observed[xv]. The following formula should be used to calculate the intensity ratio:

$$\frac{I_1}{I_2} = \frac{A_1 g_{1\lambda_2}}{A_2 g_{1\lambda_1}} e^{\left(\frac{E_2 - E_1}{KT}\right)} \qquad (1.6)$$

Calculating the non-resonance spectral line's width is another approach to ensure this. The lines are visually thin if their width is constant across all axial positions.

1.6 Calculation of electron Number Density:

1.6.1 Stark Effect:

The stark broadening, also known as the stark effect, refers to an increase in the width of the emission line profile due to an electric field's presence. The electrons and ions that are already present in the vicinity interact with the atom that is radiating, which results in the production of new radiation. The electric field that these electrons and ions produce affects the line profile because of this. As shown in figure, the stark effect leads to a thickening of the line for hydrogen and atoms that behave similarly to hydrogen[xvi].

$$n_e(cm^{-3}) = \left(\frac{\Delta\lambda^2_{FWHM}}{2\omega_s(\lambda, T_e)}\right) N_r \qquad (1.7)$$

Where Nr is the reference electron density, which subscriber of 10^{16} cm^{-3}, $\Delta\lambda^2_{FWHM}$ is the full width at the half maximum, w_s is the stark broadening parameter, and $n_e(cm^{-3})$ is the electron density.

Theoretical calculations on the broadening of spectral lines induced by the quadratic stark effect for atoms with two or more electrons are presented by.

$$\Delta\lambda_s \approx 2[1+1.75A\ (1-0.75R)]\ \omega\ \frac{N_e}{N_e^{ref}} \qquad (1.8)$$

The symbol ω stands for the electron impact half-width, the letter A stands for the ion broadening parameter, the letter N stands for the electron number density, and the letter $Nstands_e^{ref}$ stands for the reference electron number density, which is typically on the order of 10^{16} to 10^{17} cm-3. Because of the way the Stark width was measured, the lines that were selected for the number density are not completely accurate[xvii].

1.6.2 Calculations of Electron Temperature:

Calculations of the excitation temperature make up the second aspect of plasma characterization. The sample's elemental composition can be incorrectly determined if the plasma temperature is not estimated appropriately, which is necessary. The Boltzmann equation below can be used to compute the plasma temperature, i.e.

$$\ln\left(\frac{I_{ik}}{A_{ki}g_k}\right) = \frac{-1}{KT}\,E_k + \ln\left(\frac{hcN^Z}{4\pi U^Z(T)}\right) \qquad (1.9)$$

Where I_{ik} is the intensity of the transition line joining energy levels I and k, λ is the wavelength, Aki and g_k are the transition probability and statistical weight of the upper level, E_k is the energy of the upper level and U^Z (T) is the partition function, which depends on plasma temperature. A straight line results from plotting the Boltzmann equation's LHS as an Ek function[xviii]. From the equation above, the slope is equal to numerator to$\frac{-1}{KT}$. We can find the plasma temperature by calculating the slope of the line. It is important to choose the spectral lines for plotting carefully. Self-absorption should not occur in the lines, and the e

Energy in the upper levels should be substantial. Self-absorption in the spectral lines may result in incorrect temperature estimation.

1.6.3 Quantitative analysis through Calibration Free LIBS:

There are two distinct methods used in LIBS to analyze the elemental configuration. The calibration curve method is one, and the calibration-free method is another. Using calibration-free LIBS is an easy and effective technique to measure the elemental configuration[xix]. The composition of the sample can be approximated using the plasma temperature and number density, which are calculated using the Boltzmann equation and are provided as:

$$\mathbf{F}C^{Z} = \frac{U^{Z}(T)}{A_{ki}g_{k}} e^{\left(\frac{E_{k}}{KT}\right)} \qquad \textbf{(1.10)}$$

Where Aki, g_k, and E_k denote the transition probability, upper-level statistical weight, and upper energy level accordingly and CZ is the concentration of the neutral species, the intensity of the spectral line, U^Z (T) is the partition function at plasma temperature, and F is a factor the affects plasma length.

$$\mathbf{F}= \frac{L}{4\pi} \qquad \textbf{(1.11)}$$

Where L is the plasma length in the above equation. For a constant spectral system, this factor is constant. Therefore, the concentration of the neutral elements can be determined using an optically narrow spectral line of an element using the Boltzmann equation stated above.

The Saha-Boltzmann equation is utilized to determine the concentration of ionized species.

$$\frac{C^{Z+1}}{C^{Z}} = \frac{(2\pi mkT)^{\frac{3}{2}}}{n_{eh^3}} 2\frac{U_{Z+1}}{U_{Z}} e^{\frac{E_{ion}}{KT}} \qquad \textbf{(1.12)}$$

CZ+1 is the ionized species concentration, UZ+1 is its partition function, and Eion is the ionization energy. The formula for calculating each element's percentage concentration is:

$$\mathbf{\%\ E_{element}} = \frac{C_{element}}{C_{sum\ of\ elements}} \times 100 \qquad \textbf{(1.13)}$$

1.7 Line broadening:

Line broadening at specific wavelengths or frequencies affects the capacity to extract information from the spectrum numerically and qualitatively. A spectroscopic shift's line form and width can be determined using the broadening mechanics of the starting and final levels. Line shape is further impacted by additional homogeneous broadening mechanisms such as Stark, Pressure, and natural broadening. Through the use of these homogeneous broadening methods, Lorentzian form lines are produced. Gaussian line form results from inhomogeneous broadening, such as Doppler broadening. It means that both homogeneous and inhomogeneous mechanisms are affected by natural broadening. Below are a few of the physical mechanisms[xx].

1.7.1 Natural Broadening:

The most fundamental broadening line results from an isolated system atom (An atom with no external perturbation, such as electric field, pressure, or temperature)[xxi]. Heisenberg's principle can be used to explain this broadening phenomenon as follows:

$$\Delta E\, \Delta t \approx \hbar \qquad (1.14)$$

This implies,

$$\Delta v = \frac{1}{2\pi\Delta t} \qquad (1.15)$$

At a certain energy level, an electron has a specific lifetime. As seen in the equation above, an electron's energy level uncertainty can be derived from how long it spends at that level.

The spectrum tends to broaden since short lifetime levels have a significant degree of energy level uncertainty. A spectrum with a higher level of uncertainty has a wider range of frequencies. Compared to other broadening methods, the effect of the natural broadening mechanism is typically extremely small[xxii].

1.7.2 Pressure Broadening:

The broadening mostly impacts high-density materials. This broadening mechanism occurs when gas atoms transition under high pressure—these widening results from the high-pressure collision of gas atoms. Collision broadening is another name for pressure broadening. The spectral line's pressure-broadening form is Lorentzian. In a nutshell, we may say that the interaction of radiating atoms with adjacent atoms is what causes the frequency to broaden[xxiii].

1.7.3 Stark Broadening:

The homogeneous broadening mechanism's stark broadening, which is the most effective, and the system's electron radiating atom interactions are the main cause of the stark broadening. This definition demonstrates that it is strongly temperature sensitive and directly reliant on concentration or electron number density around the emitting species. Stark broadening can be used to measure electron number density (Ne). The equation for calculating a spectral line's full width at half maximum (FWHM) (i.e., stark broadening) is shown below.

$$\Delta\lambda_{1/2} = 2\omega \left(\frac{N_e}{10^{16}}\right) + 3.5A\omega \left(\frac{N_e}{10^{16}}\right)^{5/4}\left[1 - \frac{3}{4} N_D^{-1/3}\right] \qquad (1.16)$$

Stands for the impact width of an electron. A represents the ion broadening parameter.

N_e is the number density of electrons. In the Debye sphere, N_D stands for the number of particles.

The first term in the equation above depicts the result of an interaction between electrons, and the second component represents an interaction between atoms and ions. Normally, the second term in this equation is discounted because it rarely has any significant effects. Due to stark broadening, the spectral line has a Lorentzian structure.

$$\lambda_{1/2} = 2\omega \left(\frac{N_e}{10^{16}}\right) \qquad (1.17)$$

1.7.4 Doppler Broadening:

This broadening was attributed to the area around the radiating species. Doppler broadening is a term used to describe the frequency shift caused by the relative motion of the source and observer. Given that Doppler broadening is an inhomogeneous mechanism for line broadening, its line shape is Gaussian. Since atoms are always moving randomly, we can regulate the thermal motion of the atoms by adjusting the system's temperature[xxiv]. When the source (atom) moves away from the observer (detector), a slightly bigger shift in frequency is acquired in the form of a blue shift. Consequently, a change in the frequency of observed photons will occur due to the thermal disturbance of atoms.

$$\Delta\lambda_D = \lambda_0\sqrt{\frac{8kTln(2)}{m_A C^2}} \quad \textbf{(1.18)}$$

The given equation illustrates a shift brought on by relative wavelength motion, which depends on the system's temperature.

Where:

In a spectral line (m), the central wavelength is represented by λ_0

T represents the absolute temperature (K)

m_A represents the atomic mass (Kg)

k represents the Boltzmann constant (J/K)

C represents the speed of light (m/s).

Chapter 2

Experimental setup

2.1 Setup for LIBS Experiment:

Fig shows a schematic diagram for the LIBS setup to analyze the particular matter sample. Our experiment uses a 10Hz repetition rate and 5ns pulse duration Nd: YAG Q-Switched laser to light the source. This laser can produce 200mJ of energy at a wavelength of 532nm and 400mJ of energy at a wavelength of 1064nm. The pulse energy can be changed by adjusting the Q-switch delay in relation to the flash lamp source. A joule meter can be used to measure pulse energy or laser energy. With the help of a 20cm convex lens, the laser beam is focused on the sample of a particular matter sample. To rotate the sample consistently and avoid the non-uniform pits in the particulate matter sample, a 3D sample stage is utilized to place the sample in front of the laser beam. To eliminate the possibility of any breakdown in the air surrounding the sample, the particulate matter sample is positioned somewhat away from the center of focus and towards the focusing lens. Seven single laser shots were captured, each with a varied pulse delay that altered the laser's pulse energy. A fiber optic set at a right angle to the path of the laser beam is used to collect the electromagnetic radiation that the plasma plume emits[xxv].

This fiber optics field of view ranges from 0 to 45 degrees, and its core diameter is 600μm. This fiber optics was connected to a detecting device (LIBS 2000) to capture the plasma emission spectrum. The detecting system includes five distinct spectrometers, each designed to trace the emission spectra of the plasma over a particular frequency band. Each spectrometer has an optical resolution of up to 0.06nm and a slit width of 5μm. Each spectrometer has a 2048-element linear CCD array and covers a wavelength range of 200 to 700nm—the Nd: YAG laser to capture the spectrum. The laser and the detecting system were connected using a pulse generator (SRG DG 535) or a five-channel digital delay.

The software OOLIBS2000 (Ocean Optics Inc. Laser-Induced Breakdown Spectroscopy) was used to correct the emission spectra by removing the dark signals and controlling the laser beam's energy. Using the DH-2000 standard light source, the manufacturer calibrated each installed spectrometer in the LIBS2000 detection system[xxvi]. The computer program OOLIBS was used to record the plasma's spectrum for further examination.

2.1.1Schematic Diagram of LIBS:

The basics of the experiment are depicted in the figure. Below is a detailed note on each instrument installed in the LIBS experimental setup.

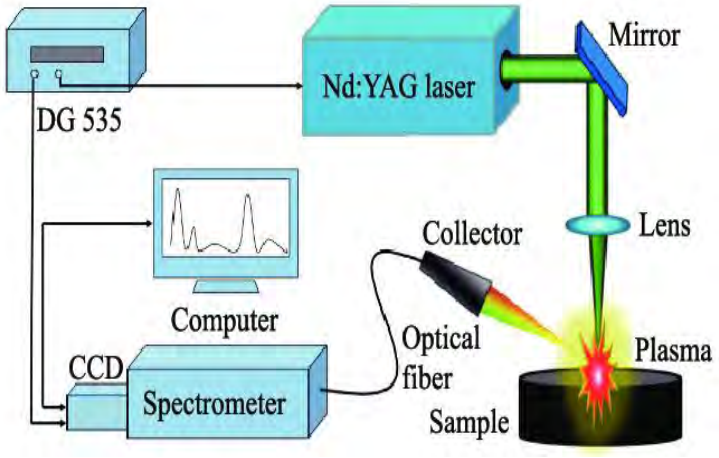

Figure 2.1 Schematic Diagram of LIBS Setup

Here is a list of equipment's we utilized in our experiment:

- Q-Switched Nd: YAG laser
- Focusing lens
- Detection System
- Triggering device
- Fiber optic cable
- Personal Computer

2.1.2 Nd: YAG Laser:

The Nd: YAG Laser is the most used solid-state laser, utilized in the LIBS experiments and numerous others. The laser's active medium is a Neodymium-doped Yttrium Aluminum Garnet Crystal. Neodymium, a dopant, alters the crystal's optical characteristics. Because the

host (YAG) and active ingredient (neodymium) have the same size, Neodymium ions modify the host (YAG) in the crystal. The positively charged Neodymium ions Nd+3 are optically pumped using the flash lamp as a source[xxvii].

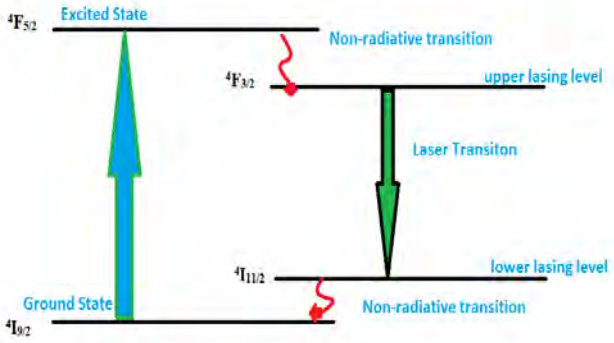

Figure 2. 2 Energy Level Diagram of Nd: YAG Crystal

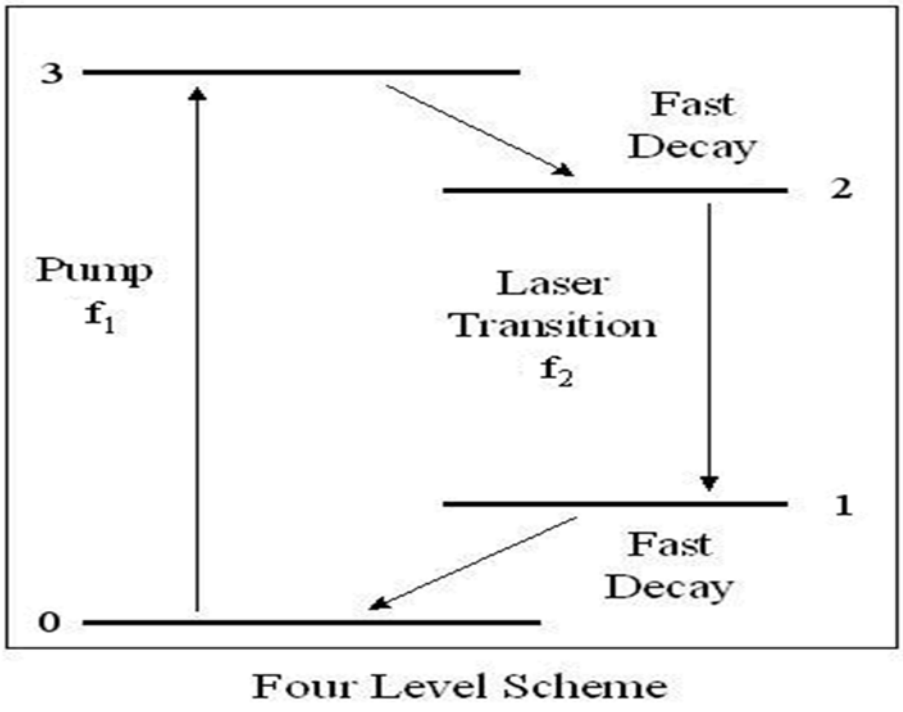

Figure 2. 3 Four-Level Energy Diagram

The four-level Nd: YAG system's energy level diagram is shown in the figure.

Neodymium's ground state atom has the electronic configuration (Xe) $4f^4 6s^2$. The J values for I^4 with L=6 and S=3/2 are 15/2, 13/2, 11/2 and 9/2, respectively, in the Russell Sounder Approximation. This means that a lower value of J will have the lowest energy. As we can see from the above diagram, the transition between the states $F^4_{3/2}$ and $I^{11/2}_4$ is generally necessary to generate a laser beam. The probability of other transitions also increases by splitting energy levels into their parts. The dominant wavelength at 300K, room temperature, and 77K, lower temperature, is 1064.8 nm and 1061.2 nm, respectively.

The slight movement in the levels of $I^4_{11/2}$ and $F^4_{3/2}$ causes the wavelength variation.

2.2.1 Detection System (LIBS 2000):

Five HD 2000-type spectrometers of high resolution make up the US 2000 detection system. These spectrometers have a resolution of roughly 0.06 nm. These 2400 or 1800 lines per millimetre gratings spectrometers cover the whole optical range. Every HR 2000 spectrometer's database was used in the software's layout. Through a data cable, the computer system and detecting system are linked so that the computer may run the OOLIBS software and acquire spectral images. When we shine a laser beam in pulse mode on a sample that is being studied, photons from the laser beam transfer their energy to the sample's atoms and become excited. After some time (roughly a few hundred nanoseconds), these excited atoms become de-excited along with the emission of radiations, which is what the spectrum on the computer screen represents. Connect the detected radiation released and send the data to the program on the computer as digital signals. Having the software OOLIBS available to capture any optical spectrum is helpful. The software's digital library can regulate every setting, gather data, and display the optical spectrum[xxviii].

The parameters of the high-resolution spectrometers used in the experiment's detection system are displayed in the table.

Table 2. 1 Specification table for the LIBS Detection System

Specification of different HR 2000 used in LIBS 2000+ Spectrometer			
Model	**Grating Lines (Lines/mm)**	**Region**	**Band Width**
LIBS HR 1	2400	Ultraviolet	200-301 nm
LIBS HR 2	2400	Ultraviolet	296-391 nm
LIBS HR 3	1800	Visible	386-513nm
LIBS HR 4	1800	Visible	619-720 nm

2.3 HR 2000 High-Resolution Spectrometer:

The resolution capabilities of a fibre optic HR 2000 spectrometer can reach 0.065 nm FWHM. The HR spectrometer measures the high-resolution lines given off by atoms or gases.

Any spectrometer's resolution is dependent on its grating and entry slit width. The HR 2000 spectrometer is a detective system from the computer system. When a laser beam contacts a sample, it creates a plasma plume of the sample in which the atoms are excited. After the atoms have been de-excited, they release radiations collected by the detection system and sent to the computer system as an electrical signal for further processing[xxix]. The data is presented and analyzed by the software OOLIBS, in the figure below, an optical worktable for the HR2000.

Figure 2. 4 High Resolution Spectrometer

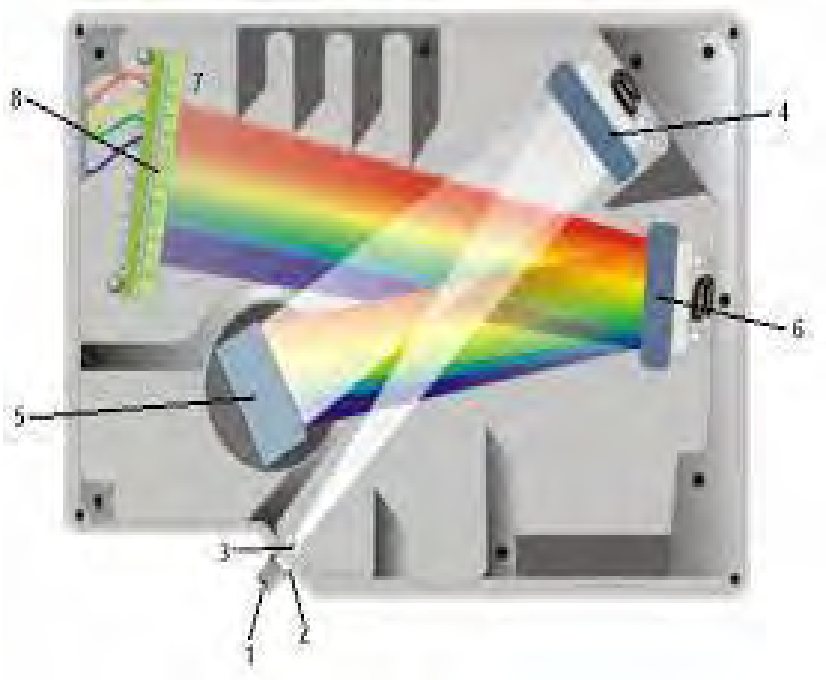

Figure 2. 5 Schematic Diagram of High Resolution Spectrometer.

A Schematic Diagram of the spectrometer is shown in the figure below.

2.3.1 SMA Connector:

An optical branch is connected to the fiber optic via an SMA connector placed at the spectrometer's entrance slit.

2.3.2 SLIT:

After passing through the SMA connector, the radiation enters the optical counter through the slit, which acts like a slit. The amount of radiation that enters the system is directly influenced by the slit's width. Our LIBS experiment used slits that were 5μm wide.

2.3.3 Absorbing Filter:

The SMA connector and this filter device are permanently attached. The filter's job is to limit the wavelengths of light that enter the detection system by blocking some specific wavelengths that fall outside the detection range of the installed spectrometers and allowing passage of wavelengths that fall inside that range.

2.3.4 Collimating Mirror:

The purpose of the collimating mirror is to reflect incident radiations towards a grating system from an entrance slit. Collinear rays are reflected from the incident radiation by the collimating mirror.

2.3.5 Grating:

Collinear beam diffracts after passing through the grating system and collimating mirror reflection. The grating (lines/mm) of each spectrometer in the detecting system varies from 1800 to 2400, each with unique specifications. The grating arrangement virtually completely and accurately covers the entire light spectrum.

2.3.6 Focusing Mirror:

The focusing mirror's job is to point the spectrum in the direction of the detector.

2.3.7 Detector Collection lens:

A large-diameter cylindrical lens is required to capture the largest possible portion of the radiation spectrum that has been gathered. In principle, this lens directs radiation properly and concentrates it on the detector.

2.3.8 CCD Detector:

The CCD detector is the detection system's most crucial and significant component. Each pixel in the detecting system responds solely to a particular wavelength when radiation strikes the detector, constructed of a 2048-element linear CCD array.

Chpater#3

Results and Discussion

An Nd: YAG utilized in our experiment had a frequency source for plasma formation to investigate the emission emanating from the laser-produced plasma on the surface of the particulate matter sample. The Q switched Nd: YAG Laser utilized in our experiment had a frequency of 10 Hz and operated at a wavelength of 532 nm through second harmonic generation (SHG) at 532 nm and a time delay of 10μs at lase energy of 34.4mJ. A convex lens with a 10cm focal length was utilized to concentrate the pulsed laser beam on the particulate matter sample using the laser as externally triggered. The target surface's distance from the focusing lens is adjustable using a mobile microscope with a convex lens installed. The fiber optic is mounted on an adjustable stage that moves towards the plasma point. Through the fiber optic, the HR2000 spectrometer was connected to the laser-ablated plasma emission. The computer has received the recorded data from the spectrometer along with the lines of emission from the laser-induced plasma. The emission lines were captured at a right angle to the incoming laser beam and come from the DPM sample plasma that the laser beam has created[xxx].

3.1.1 Particulate Matter and Sample Preparation:

Petrol Particulate Matter was obtained from miscellaneous in-use petrol engine passenger vehicles of diverse types and models from major brand car producers. PPM sample was collected from Petrol petrol-powered passenger vehicle that was in use and came from a well-known automaker. A vehicle from a production model that is often seen on public roads was chosen for the sample collection. Neither a prototype nor a test engine was utilized. It is important to note that the technical setup and characteristics of the specific vehicle have not been the focus of these investigations. Additionally, we have not measured the mineral composition of engine intake air or the particles adhered due to the air filter of the vehicle thus the air pollution hasn't been taken into account. Because the vehicle has been operating in many environments throughout their lives, it would be difficult to analyze both situations. Petrol particulate matter has been removed from the passenger vehicle tailpipe end portion. Specifically, it can be collected from the

particulate filter that is designed to trap and remove particulate matter from the exhaust gases. The results from this study come from the PPM matrix in terms of the LIBS spectrum[xxxi]. The goal is to use laser-induced breakdown spectroscopy to qualitatively and quantitatively describe the elements that make up this matrix. Analysis of the major spectral lines that are most prominent in the ultraviolet, visible, and infrared optical emission spectrum from petrol particulate matter is given specific attention. The collected petrol-engine exhaust particles were collected on filter paper. After that LIBS performed an analysis on the PPM sample without further preparation[xxxii]

3.1.2 Spectrum Analysis:

The classified spectrums of the particulate particles are shown in the figures. This figure 8 displays the complete spectrum in the wavelength range of 235-715nm, which displays both strong and weak emission lines consisting of the elements lithium (Li), Hydrogen (H), Sodium (Na), Calcium (Ca), Iron (Fe), and Carbon (C) as we as multiplet cluster of singly ionized magnesium (Mg ii)

Because of 3P2 P1/2,3/2→3S2S1/2 and 3d2 D3/2,5/2→3p2P1/2,3/2 transitions, the spectrum was separated into sections in order to have a clear understanding of the spectrum due to the large number of spectral lines. In the table 1.2 the wavelength of all the emission lines of the emission spectrum of the particulate matter sample is classified, which shows that Ca and Fe have the major lines in the spectrum. These lines were identified from proper checking while using the NIST database.

The presence of Ca, Fe, Na, Cu, Ni, Li, and Mg is confirmed by spectral lines. Na, Li, and Cu are trace elements, while Ni is a minor chemical element. However, the intensity and number of lines for Ca, Na, Mg, and Fe show that these are the major elements present in the sample.

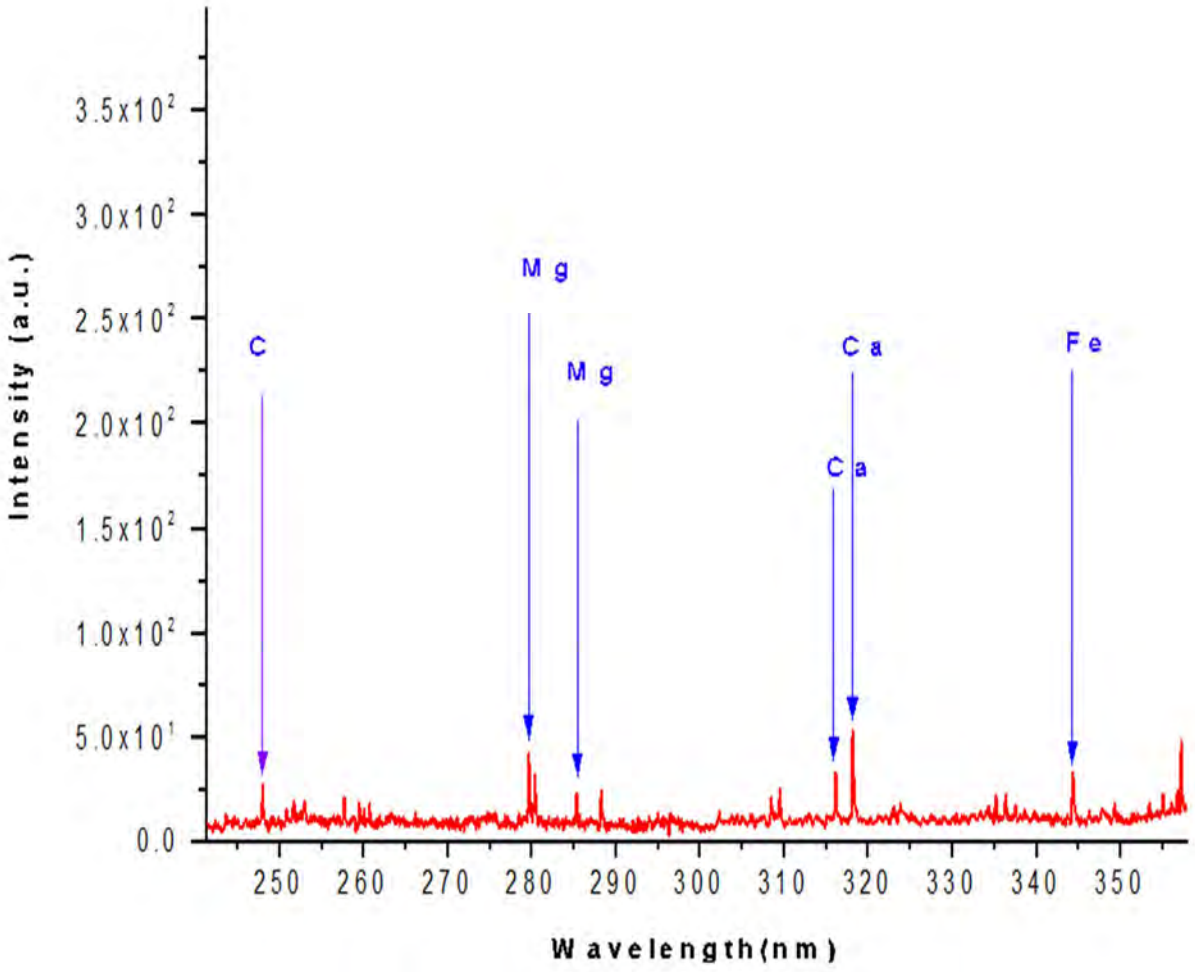

Figure 3. 1 Classified emission spectrum of PPM covering the spectral range for 240-355 nm at energy of 34.5 mJ.

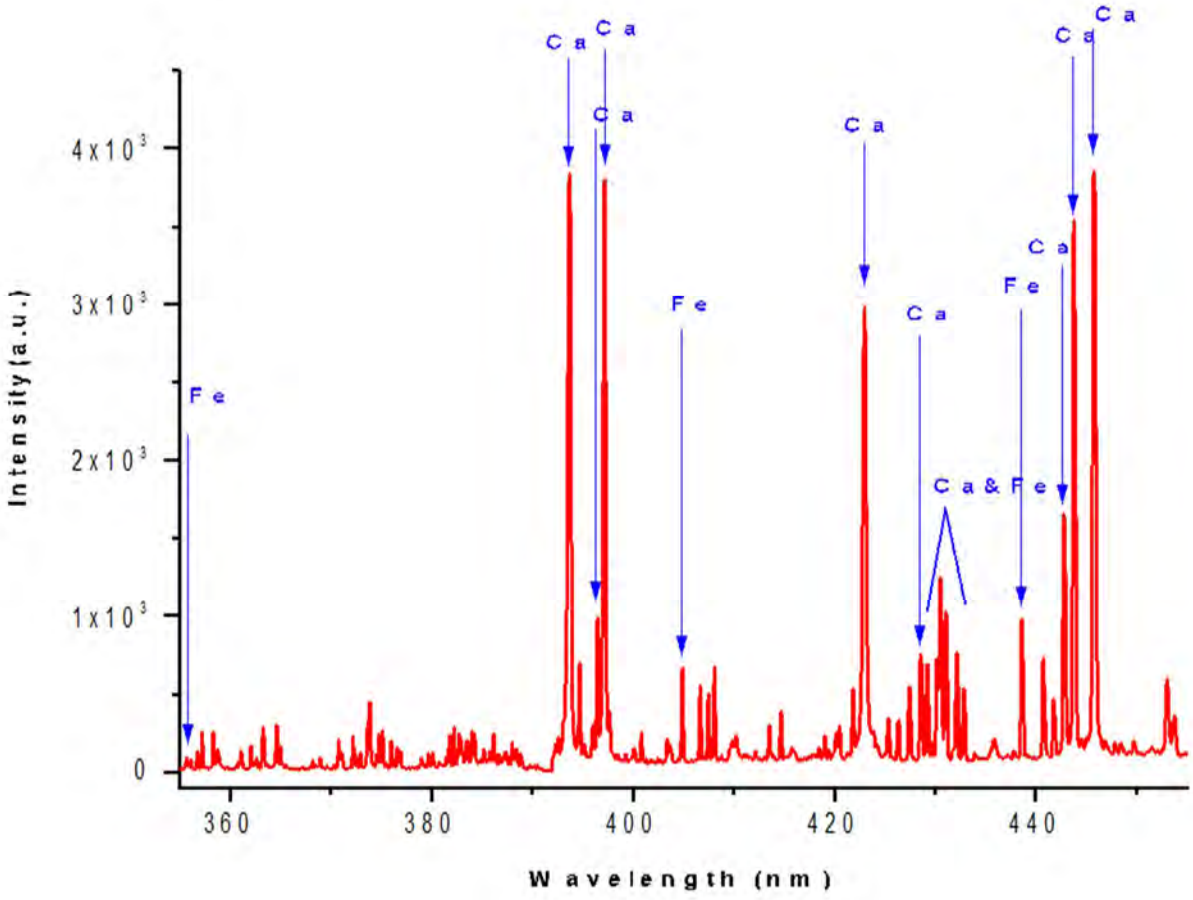

Figure 3. 2 Classified emission spectrum of PPM covering the spectral range for 355-455 nm at energy of 34.4 mJ.

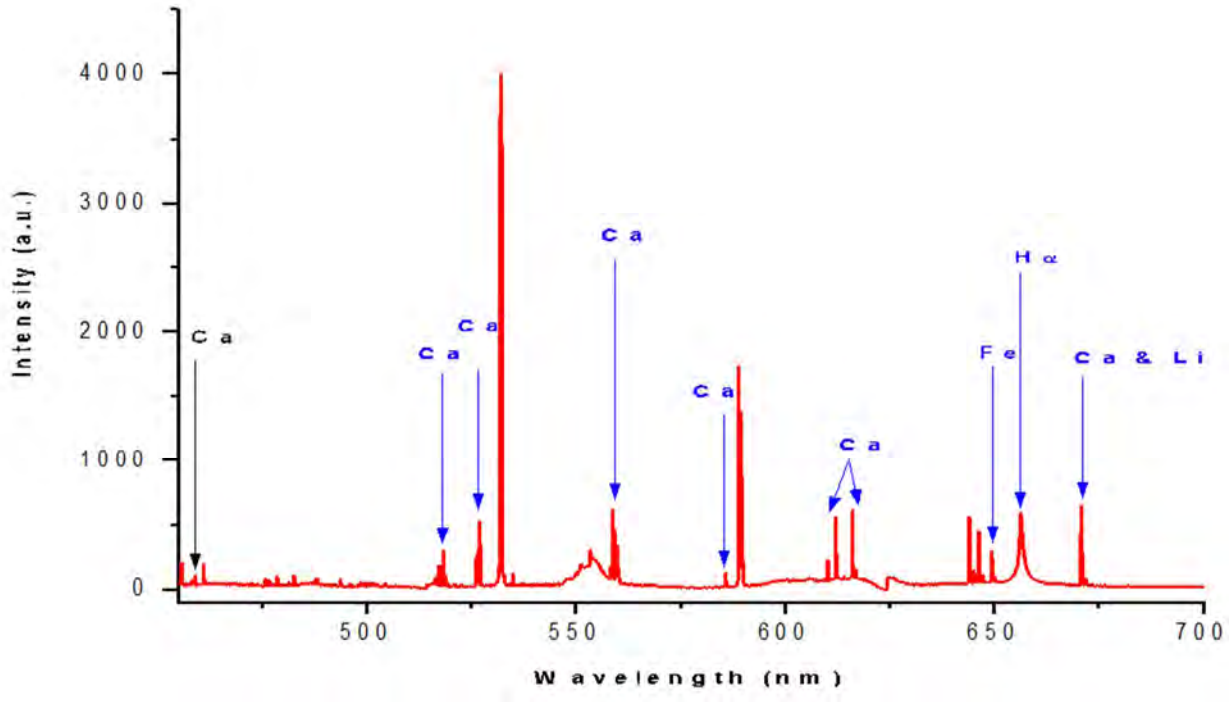

Figure 3. 3 Classified emission spectrum of PPM covering the spectral range for 455-700 nm at energy of 34.4 mJ

Table 3. 1 Significant no of emission lines were formed in the emission spectrum of PPN

Elements	Wavelengths
Hydrogen(H)	656.26 (H_α)
Carbon(C)	247.9
Sodium(Na I)	588.94, 589.54
Lithium (Li I)	670.78, 610.21
Magnesium(Mg I)	285.28, 517.25, 518.36,
Magnesium(Mg II)	279.59, 280.34
Calcium (Ca I)	316.08, 318.12, 397.85, 422.90, 428.52, 429.17, 429.66, 430.13, 430.48, 431.00, 442.76, 443.74, 445.72, 339.57, 396.85, 441.73, 504.37, 518.36, 518.86, 526.18, 526.54, 527.00, 534.92, 558.81, 558.13, 559.37, 559.78, 585.70, 616.14, 616.86, 644.01, 645.08, 646.34, 647.25, 671.77
Calcium (Ca II)	393.57, 396.85
Iron (Fe I)	344.59, 344.26, 259.99, 361.07, 362.06, 363.31, 364.64, 364.97, 427.40, 425.28, 425.30, 375.99, 376.55, 376.88, 368.19, 368.94, 370.76, 371.11, 372.17, 372.43, 373.87, 372.99, 376.55, 381.74, 382.19, 400.74, 403.30, 404.81, 406.58, 407.38, 408.00, 438.58, 522.70, 523.27
Nickel (Ni I)	352.81, 352.33, 351.59, 341.51

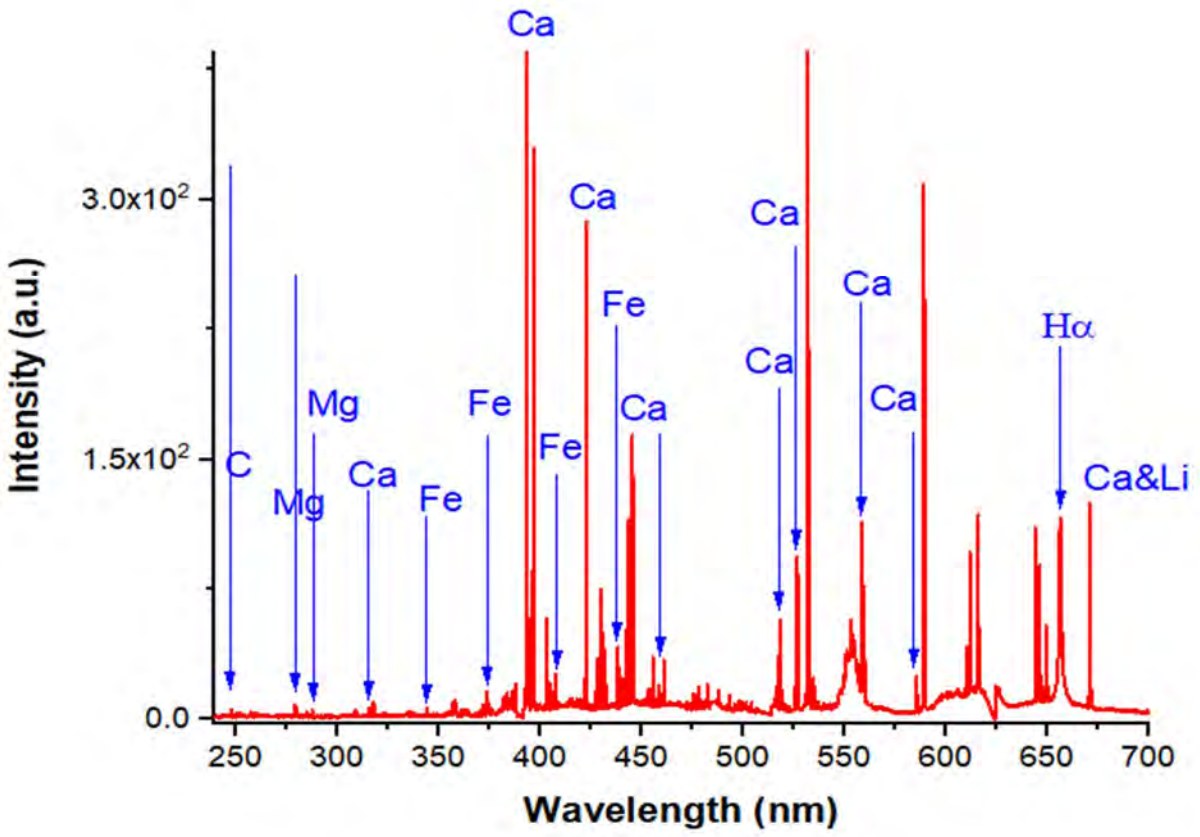

Figure 3. 4 Classified emission spectrum of PPM covering the spectral range for 240-700 nm at energy of 34.4 mJ.

3.1.2 Electron Number Density:

The electron number density can be determined using the stark broadening width of particular lines in the spectrum that neutral atoms or ions emit. We select the interference–free spectral lines since they produce some appropriate results.

Since the plasma satisfies the requirements for thermodynamic equilibrium, we use stark broadening of the Ha line to measure the electron number density[xxxiii]. This is because not all spectral lines are well-isolated lines having precise sharp broadening parameters. The lowest electron number density in local thermodynamic equilibrium is determined by a relation [1.5].

$$N_e \geq 1.6 \times 10^{12} \sqrt{T_k} \, (\Delta E_{ev})^3 \qquad (3.1)$$

3.1.3 Stark Broadening Method:

In our work the electron number density in the plasma generated by the 532nm wavelength of the Nd: YAG is calculated by using the stark broadening parameter of the Ha line at 656.27 nm. The equation for calculating a spectral line from the full width at half maximum or Stark broadening is stated as by the following equation, which represents stark broadening, which is used to determine a spectral line of full width at half maximum (FWHM) [38].

$$\Delta\lambda_{1/2} = 2\omega \left(\frac{N_e}{10^{16}}\right) + 3.5A\omega \left(\frac{N_e}{10^{16}}\right) \qquad (3.2)$$

In this case, A, Ne, and ND stand for, respectively, electron impact parameter, ion broadening parameter, electron number density, and Debye Sphere particles. The interaction between the ions and atoms accounts for the second part of the equation above. Since the influence of the ion atom interaction is typically negligible we may disregard it and use only one equation to determine the electron number density in Cm-3 which is as follows:

$$N_e = 1017 \times \left(\frac{\Delta\lambda_{1/2}}{1.09\ 8}\right)^{1.47235} \qquad (3.3)$$

The spectral line shape profiles have Lorentzian characteristics. Fig. 10 Displays the Lorentzian-Fitting Ha Spectral line peaks obtained at 89mJ of Nd: YAG laser energy.

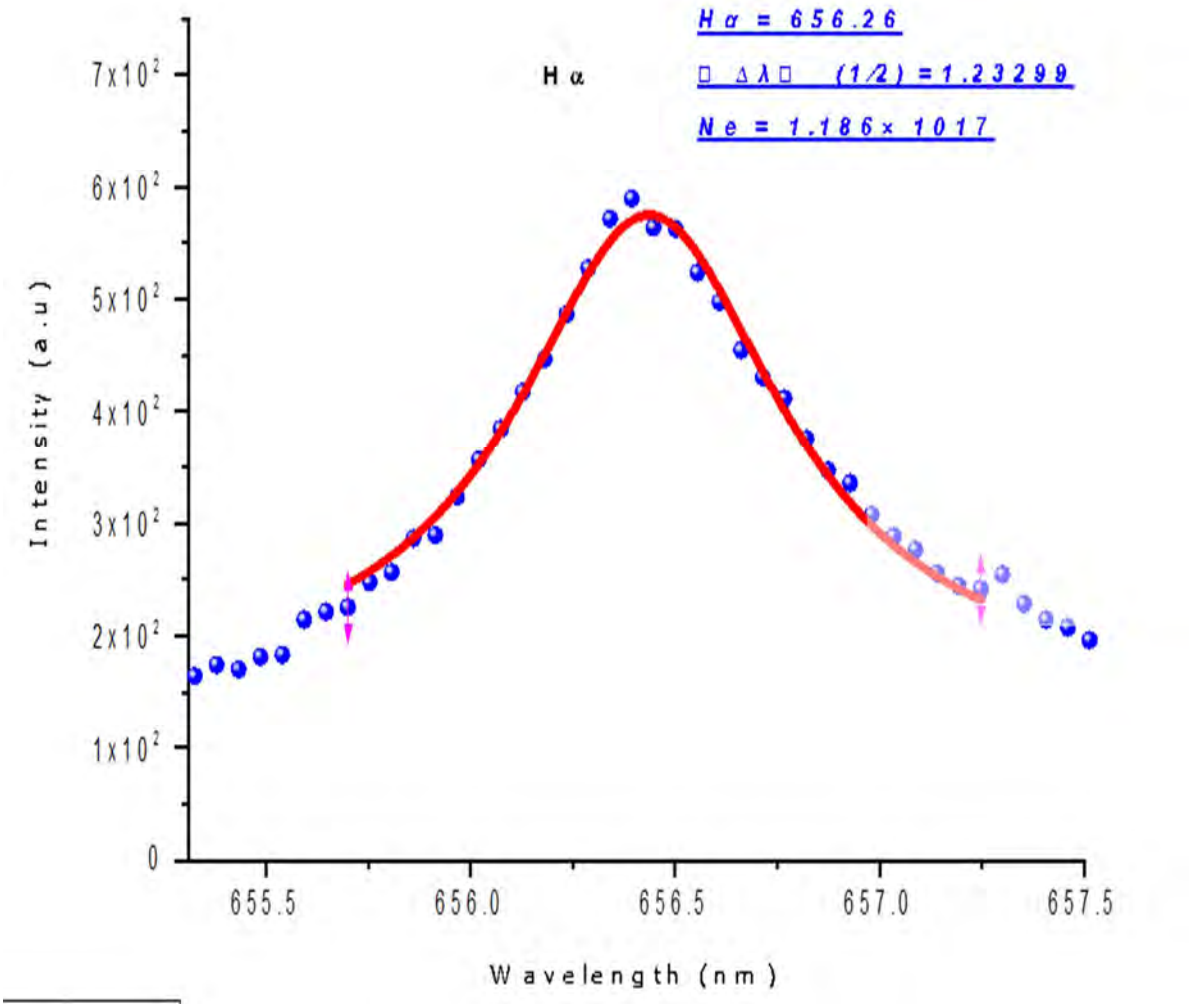

Figure 3.5 Lorentzian fitting of spectral line 656.26 nm**.**

By following equation 3.3 we calculated electron number density for the SP LIBS spectrum by using the FWHM of Ha line.

$$Ne = 10 \times (\Delta\lambda_{1/2}/1.098)$$

Where $\Delta\lambda_{1/2}$ = FWHM = 1.23299

$$(1.12294)^{1.47235}$$

$$Ne = 10^{17} \times (1.186157)$$

$$Ne = 1.186 \times 10^{17}\ cm^{-3}$$

3.2 Local Thermo Dynamical Equilibrium (LTE) Condition:

For the optical plasma to be in local thermo dynamical equilibrium (LTE) the ionic and excitation temperatures need to be similar to the electron temperature. In recent years several tests have been made to verify the existence of thermo dynamical equilibrium in plasma[xxxiv]. A minimal value of the electron density was proposed to ensure that collisions predominate the population of levels, which would demonstrate the existence or absence of Thermo dynamical equilibrium.

To confirm that the plasma is in LTE, Mc Whirter suggested using a foundation for a trivial limit of the electron number density.

$$\mathbf{N_e \geq 1.6 \times 10^{17} (\Delta E)^3 (T)^{1/2}} \qquad \mathbf{(3.4)}$$

Where T is the excitation temperature in kelvin (K) and E (eV) is the maximum transition energy from an upper to a lower ground level (n→m). For measuring the LTE condition we have selected the line of Ca-1 at 616.21 to check whether the plasma is in LTE condition or not.

Table 3. 2 Illustrate the Ca-1 at 616.21 for the LTE condition.

Symbol	λ (nm)	T(K)	$T^{1/2}$	E(eV) (Lower)	E(eV) (Upper)	ΔE (eV)	$(\Delta E)^3$	$N_e \geq 1.6 \times 10^{17} (\Delta E)^3 (T)^{1/2}$
Ca-I	616.21	8700	93.27	1.89	3.91	2.02	8.13	1.23×10^{20}

The approximate electron number density of the sample is ($1.23 \times 10^{15} cm^{-3}$) calculated from the stark broadening lines is greater than the number density measured by using the Mc Whirter criterion. Therefore it can be concluded that plasma is satisfying the LTE condition.

3.3 Optically Thin Plasma Condition:

To examine the laser-induced plasma spectroscopically, two parameters must be satisfied. This first is the LTE requirement and the second is that the plasma had to be optically thin. We compare the theoretical line intensities with those calculated from the provided equation to determine if the plasma is optically thin or not Fig.

$$\frac{I_1}{I_2} = \frac{A_1 g_1 \lambda_2}{A_2 g_2 \lambda_1} e^{-\left(\frac{E_2 - E_1}{KT}\right)} \qquad \textbf{(3.5)}$$

Here I_1 and I_2 stand in for the observed emission line intensities, while λ_1 and λ_2 are their wavelengths. The transition probabilities are represented by A1 (s^{-1}) and A2 (s^{-2}). g_1 and g_2 are the statistical weights and E_1 and E_2 (eV) represent the upper and lower energies of these observed transitions. To determine the intensity ratios, we used the sample's Ca-1 emission lines at 428.3nm and 429.89nm. The right-hand side of this relation is the theoretical value that uses the parameters catalog in the NIST database.

Table 3.3 Illustrates the optically thin Plasma Condition.

Wavelength (nm)	**Element**	**Probability** $A \times 10^7$ (S^{-1})	**E(ev)**	**g=2j+1**	$A_1 g_1 \lambda_2$	$A_2 g_2 \lambda_1$	$\frac{A_1 g_1 \lambda_2}{A_2 g_2 \lambda_1} \times exp\ -(\frac{E_{2-E_1}}{KT_e})$
428.93	Ca-I	6×10^7	4.76	3	77.38	95.14	0.8133
429.89	Ca-I	4.66×10^7	4.76	3	6.009	7.738	0.7765

Therefore, RHS of the equation is a theoretical value which is $\frac{I1}{I2}$ = 0.7748. The approximate ratio of the intensities is $\boldsymbol{\frac{I1}{I2} = 0.8296}$.

The experimental and theoretical intensities ratios for the sample are comparable with 5%.

3.4 Boltzmann Plot for measuring Plasma Temperature:

The electron temperature of the plasma is calculated using the Boltzmann plot method, which is frequently used to analyze spectroscopic data. This method compares the relative intensities of two or more lines in the spectra with relatively large energy differences to determine the electron temperature of the plasma. To properly use the Boltzmann plot method to quantity T_e, the excitation level must be obtained in an LTE scenario[xxxv]. However, the Boltzmann plot equation that is used in the data analysis is:

$$\frac{N_j}{N_i} = \frac{g_j}{Z(T)} e^{-\frac{E_j}{KT_e}} \qquad \textbf{(3.6)}$$

g_j and g_i represent the two level's statistical weights.

K is the Boltzmann Constant

$_e$ is Plasma temperature$\frac{N_j}{N_i} = \frac{g_j}{Z(T)} e^{-\frac{E_j}{KT_e}}$

Z (t) is the partition function:

$$\mathbf{Z\,(t) = \sum m g_m\, e^{-\frac{E_j}{KT_e}}}$$

The emission intensity of this emission line can be expressed as a state function.

$$\mathbf{I_{ji} = \frac{hc}{4\pi\lambda_{ji}} A_{ji}\, N_j}$$

A_{ji} is the emitted light's wavelength.

h is Planck's constant.

C the vacuum speed of light

A_{ij} is the transition probability.

By substituting this equation in Eq 3.3 the resulting expression is

$$\mathbf{\frac{\lambda_{ij}}{g_i} A_{ji} = \frac{hc}{4\pi\lambda_{ji}} A_{ji}\, N_j}$$

By taking the logarithm on both sides of the equation after we get:

$$\mathbf{\ln\left(\frac{I_{ji}\,\lambda_{ji}}{g_j A_{ji}}\right) = -\frac{Ej}{KT_e} + C} \qquad \mathbf{(3.7)}$$

Where $C = \ln \frac{hcN}{4\pi Z(T)}$

Which indicate a straight-line equation. The slope of the straight line that is shown between energy and formula on the left side of equation 3.7 can be used to compute the electron temperature (Te).

We will only pick the lines that are well separated/isolated, un-saturated, and spectrum at an energy of 34.4mJ in order to determine plasma temperature. Table-5 lists the spectral lines wavelengths and other pertinent information needed to determine the electron temperature.

Table 3. 4: Illustrates the measured spectral lines for the Boltzmann plot

Symbol	**Wavelength (nm)**	**Statistical Weight g = 2J+1**	**Transition Probability A_{ji}**	**Intensity I**	**Energy of upper state cm^{-1}**	$\frac{I_{ji}\lambda_{ji}}{g_i A_{ji}}$
Ca I	430.774	1	0.41438	800.46	38417.543	20.71917
Ca I	442.544	3	0.41762	738.02	37748.197	20.88079
Ca I	443.496	5	0.41643	1516.18	37751.867	20.82142
Ca I	504.162	3	0.41154	277.35	41679.008	20.57702
Ca I	527.027	5	0.425	1762.78	39340.08	21.24975
Ca I	612.222	3	0.43617	1167.56	31539.495	21.80873
Ca I	616.217	1	0.43152	1379.35	31539.495	21.57588
Ca I	646.257	7	0.42019	1338.93	35818.713	21.00936
Ca I	647.166	7	0.43471	476.88	35818.713	21.73554
Ca I	431.865	3	0.41143	720.28	38464.808	20.57147

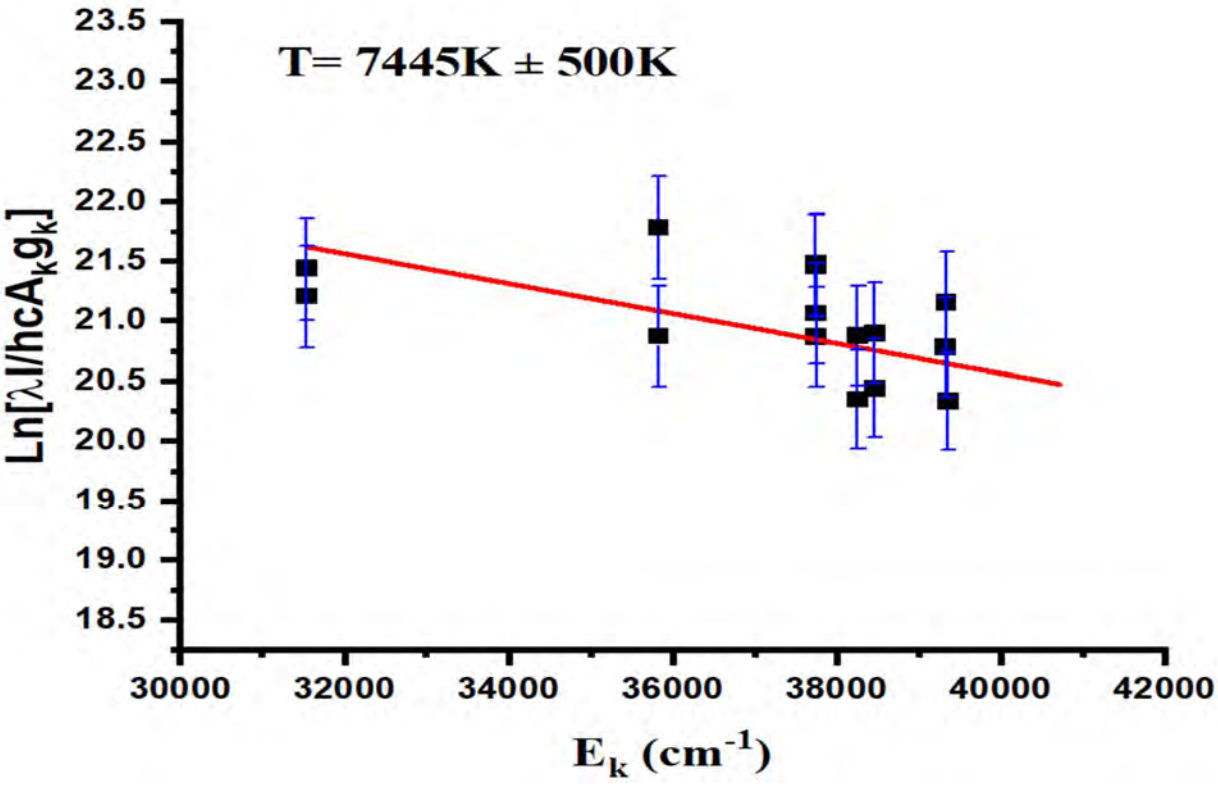

Figure 3.1 Boltzmann plot of Ca-I spectral lines.

Figure 11 illustrates the Boltzmann plot of the spectral lines of Ca-I shown in Table 5. The calculated plasma temperature of the LIBS spectrum is:

$$T_e = 7445 \text{ K}$$

3.5 Quantitative Analysis through Calibration Free Method:

The one-line calibration free (CF-LIBS) approach has been used to determine the composition of the elements for the Particulate matter sample by using the average values of electron densities and plasma temperatures in the Saha-Boltzmann equation. The following Boltzmann equation was used to calculate the neutral atom concentration.

$$FC^Z = \frac{I_k U^Z(T)}{A_{kg_k}} e^{-\frac{E_k}{KT}}$$

three here F represents the ablated mass, **C_Z** is related to the composition of the neutral atom, **I_k** is related to the line intensity, **g_k** represents the statistical weight of the upper-level transition; **A_k** related to the transition probability, **UZ (T)** is the partition function, **E_k** is the upper energy level, T is the Plasma temperature and K is the Boltzmann constant. The construction of the ionized atoms C_{Z+1} for the elements was measured by using the following **Saha-Boltzmann equation**[xxxvi].

$$\frac{n_e C^{Z+1}}{C^Z} = \left(\frac{\left(\sqrt[3]{2m_e KT}\right)}{h^3}\right) 2 \frac{U_{Z+1}}{U_Z} e^{\frac{-Eion}{KT}} cm^{-3} \qquad (3.8)$$

The amount of how much element is present in the sample is the sum of the neutral and ionic contributions.

$$C^{\alpha}{}_T = C^{\alpha}{}_Z + C^{\alpha}{}_{Z+1} \qquad (3.9)$$

The percentage composition of the element has been calculated using the relationship:

$$C_{\%} = C^{\alpha}{}_T / C_T \times 100 \qquad (3.10)$$

CαT represents the composition of each element, and CT represents the sum of the compositions of all elements present in the sample. The spectroscopic parameters of the spectral lines were selected to measure the concentrations from the NIST database ("NIST database", 2023). The results of how much concentration of elements are in the sample are listed in Table 6.

Table 3. 5

Fe%	Ca%	C%	Mg%	Li%	Na%	Ni%	Cu%	H%
89.99	4.76	4.06	0.13	0.03	0.06	0.93	0.01	0.03

3.6 Conclusion

In this study, a LIBS method for precise qualitative and quantitative analytical analyses of PPM is proposed. PPM sample was collected from a Petrol-powered passenger vehicle that was in use and from a well-known automaker. We discovered from LIBS analysis that PPM from in-use automobiles does not mostly contain pure carbon particles. Instead, it is mainly composed of several chemical elements in varying quantities. Major chemical elements in the PPM matrix can be measured instantaneously using the high-resolution LIBS approach.

From qualitative LIBS measurements, we discovered the major PPM compounds: Carbon (C), Iron (Fe), Magnesium (Mg), and Calcium (Ca) elements. Instead of major elements, we have also discovered the trace and minor elements Lithium (Li) and Nickel (Ni). A special concern of this research has been given to the quantification analysis of the LIBS signal obtained from the different PPM matrices. We have characterized quantitatively the PPM sample and its main elemental compositions. We are using a high-resolution LIBS approach. In this work, we evaluated the qualitative and quantitative composition of the major chemical constituents in the PPM matrix. However, further research will need to gather specific data on other significant elements present in PPM that could not be detected, specifically the amounts of Sulphur and chlorine[xxxvii].

The spectral window gap in our current LIBS configuration is the cause for this. Minor and trace components in PPM are of additional interest. Furthermore, we would like to compare the Particulate matter of diesel and petrol engines to check which elements are present in the patrol-running vehicles. A general understanding of PPM and its chemistry can help control combustion, Petrol exhaust emissions, and Petrol engines. Therefore, in the future, it will be essential to further aid in controlling and restricting undesirable pollutant emissions from Petrol-engine driven vehicles in actual driving scenarios. This will be accomplished by developing the in-situ LIBS technique for particulate matter. However, in addition to Petrol fuel, fuel additives, and lubricating oils, after-treatment devices like PPF, DOC, or catalytic converters can also impact the ultimate PM emission composition from petrol-engine vehicles. As a result, it would be crucial first to evaluate specific parts and traces from these devices to understand and

differentiate between the proportion of chemical elements and composition in the final PM matrix and the emissions from petrol engines. This information may be used to comply with new emission standards and laws.

References

[i] El'yashevich, M. A., Kembrovskaya, N. G., & Tomil'chik, L. M. (1990). Rydberg and the development of atomic spectroscopy (Centennial of JR Rydberg's paper on the laws governing atomic spectra). *Soviet Physics Uspekhi*, *33*(12), 1047.

[ii] Williams, D. A., & Herbst, E. (2002). It's a dusty Universe: surface science in space. *Surface Science*, *500*(1-3), 823-837.

[iii] Scholz, E. (2006). Introducing groups into quantum theory (1926–1930). *Historia mathematica*, *33*(4), 440-490.

[iv] Colegrove, F. D., & Franken, P. A. (1960). Optical pumping of helium in the s 1 3 metastable state. *Physical Review*, *119*(2), 680.

[v] Marcelli, A., Cricenti, A., Kwiatek, W. M., & Petibois, C. (2012). Biological applications of synchrotron radiation infrared spectromicroscopy. *Biotechnology advances*, *30*(6), 1390-1404.

Al-Ali, T. M., Albakry, A., & Razvi, M. A. N. Spectroscopic Analysis of Plastic samples Using Laser Induced Breakdown Spectroscopy.

[vi] Ngo, T. D., Kashani, A., Imbalzano, G., Nguyen, K. T., & Hui, D. (2018). Additive manufacturing (3D printing): A review of materials, methods, applications and challenges. *Composites Part B: Engineering*, *143*, 172-196.

[vii] De Giacomo, A., Dell'Aglio, M., Gaudiuso, R., Amoruso, S., & De Pascale, O. (2012). Effects of the background environment on formation, evolution and emission spectra of laser-induced plasmas. *Spectrochimica Acta Part B: Atomic Spectroscopy*, *78*, 1-19.

[viii]Zeng, H., Du, X. W., Singh, S. C., Kulinich, S. A., Yang, S., He, J., & Cai, W. (2012). Nanomaterials via laser ablation/irradiation in liquid: a review. *Advanced Functional Materials*, *22*(7), 1333-1353.

[ix]Larsen-Freeman, D. (1997). Chaos/complexity science and second language acquisition. *Applied linguistics*, *18*(2), 141-165.

[x] Schutze, A., Jeong, J. Y., Babayan, S. E., Park, J., Selwyn, G. S., & Hicks, R. F. (1998). The atmospheric-pressure plasma jet: a review and comparison to other plasma sources. *IEEE transactions on plasma science*, *26*(6), 1685-1694.

[xi] Gardette, V., Motto-Ros, V., Alvarez-Llamas, C., Sancey, L., Duponchel, L., & Busser, B. (2023). Laser-induced breakdown spectroscopy imaging for material and biomedical applications: recent advances and future perspectives. *Analytical chemistry*, *95*(1), 49-69.

[xii] Gigosos, M. A., & Cardenoso, V. (1987). Study of the effects of ion dynamics on Stark profiles of Balmer-α and-β lines using simulation techniques. *Journal of Physics B: Atomic and Molecular Physics*, *20*(22), 6005.

[xiii] Tognoni, E., Cristoforetti, G., Legnaioli, S., & Palleschi, V. (2010). Calibration-free laser-induced breakdown spectroscopy: state of the art. *Spectrochimica Acta Part B: Atomic Spectroscopy*, *65*(1), 1-14.

[xiv] Howell, J. R., Mengüç, M. P., Daun, K., & Siegel, R. (2020). *Thermal radiation heat transfer*. CRC press.

[xv] Malik, A. K., Montarde, P., & Haines, M. G. (2000). Spectroscopic measurements on xenon plasma in a hollow cathode. *Journal of Physics D: Applied Physics*, *33*(16), 2037.

[xvi] El Sherbini, A. M., Hegazy, H., & El Sherbini, T. M. (2006). Measurement of electron density utilizing the Hα-line from laser produced plasma in air. *Spectrochimica Acta Part B: Atomic Spectroscopy*, *61*(5), 532-539.

[xvii] Konjevic, N., & Roberts, J. R. (1976). A critical review of the Stark widths and shifts of spectral lines from non-hydrogenic atoms. *Journal of Physical and Chemical Reference Data*, *5*(2), 209-257.

[xviii] CARLETON III, F. E. (1970). *Flow Patterns in a Confined Plasma Jet*. University of Michigan.

[xix] Singh, V. K., & Rai, A. K. (2011). Prospects for laser-induced breakdown spectroscopy for biomedical applications: a review. *Lasers in medical science*, *26*, 673-687.
[xx] Manceau, J. M., Biasiol, G., Tran, N. L., Carusotto, I., & Colombelli, R. (2017). Immunity of intersubband polaritons to inhomogeneous broadening. *Physical Review B*, *96*(23), 235301.
[xxi] Stoneham, A. M. (1969). Shapes of inhomogeneously broadened resonance lines in solids. *Reviews of Modern Physics*, *41*(1), 82.
[xxii] Konjević, N. (1999). Plasma broadening and shifting of non-hydrogenic spectral lines: present status and applications. *Physics reports*, *316*(6), 339-401.
[xxiii] Wall, E. L. (2016). A STUDY OF THE FUNDAMENTAL ORIGIN OF THE DIMENSIONS OF THE BOHR RADII OF THE HYDROGEN ATOM AS DETERMINED BY THE QUANTIZED DYNAMIC ELECTRIC FIELD SURROUNDING A VORTEX MODEL OF THE ELECTRON. *Hadronic Journal*, *39*(1).
[xxiv] Xiao, Y. (2009). Spectral line narrowing in electromagnetically induced transparency. *Modern Physics Letters B*, *23*(05), 661-680.
[xxv] Tu, J., Miyamoto, I., & Inoue, T. (2002). Characterizing keyhole plasma light emission and plasma plume scattering for monitoring 20 kW class CO 2 laser welding processes. *Journal of laser applications*, *14*(3), 146-153.
[xxvi] Abrar, M., Iqbal, T., Fahad, M., Andleeb, M., Farooq, Z., & Afsheen, S. (2018). Determination of hazardous ingredients in personal care products using laser-induced breakdown spectroscopy. *Laser Physics*, *28*(5), 056002.
[xxvii] Zagumennyi, A. I., Mikhailov, V. A., & Shcherbakov, I. A. (2021). Rare-Earth Ion Lasers—Nd3+. In *Handbook of laser technology and applications* (pp. 35-53). CRC Press.
[xxviii] Bashir, S., Dawood, A., Hayat, A., Askar, S., Ahmad, Z., Ahmad, H., & Khan, M. A. (2023). Laser-assisted plasma formation and ablation of Cu in a controlled environment. *Heliyon*, *9*(8).
[xxix] Solé, J., Bausa, L., & Jaque, D. (2005). *An introduction to the optical spectroscopy of inorganic solids*. John Wiley & Sons.
[xxx] Thomas, N., Hussmann, H., Spohn, T., Lara, L. M., Christensen, U., Affolter, M., ... & Metz, B. (2021). The BepiColombo laser altimeter. *Space science reviews*, *217*, 1-62.
[xxxi] Maricq, M. M. (2007). Chemical characterization of particulate emissions from diesel engines: A review. *Journal of Aerosol Science*, *38*(11), 1079-1118.
[xxxii] Kautkar, N. U., & Premkartikkumar, S. R. (2022). An impact of emulsified cottonseed biodiesel with Nano additives on low heat rejection engine. *Environment, Development and Sustainability*, 1-20.
[xxxiii] Cvejić, M., Dzierżęga, K., & Pięta, T. (2015). Investigation of thermodynamic equilibrium in laser-induced aluminum plasma using the Hα line profiles and Thomson scattering spectra. *Applied Physics Letters*, *107*(2).
[xxxiv] Cristoforetti, G., De Giacomo, A., Dell'Aglio, M., Legnaioli, S., Tognoni, E., Palleschi, V., & Omenetto, N. (2010). Local thermodynamic equilibrium in laser-induced breakdown spectroscopy: beyond the McWhirter criterion. *Spectrochimica Acta Part B: Atomic Spectroscopy*, *65*(1), 86-95.
[xxxv] Hahn, D. W., & Omenetto, N. (2010). Laser-induced breakdown spectroscopy (LIBS), part I: review of basic diagnostics and plasma–particle interactions: still-challenging issues within the analytical plasma community. *Applied spectroscopy*, *64*(12), 335A-366A.
[xxxvi] He, G. C., Sun, D. X., Su, M. G., & Dong, C. Z. (2011). A quantitative analysis of elements in soil using laser-induced breakdown spectroscopy technique. *The European Physical Journal Applied Physics*, *55*(3), 30701.
Miller, B., Dugwell, D. R., & Kandiyoti, R. (2003). The influence of injected HCl and SO2 on the behavior of trace elements during wood-bark combustion. *Energy & fuels*, *17*(5), 1382-1391. [xxxvii]